ADVANCED MATERIALS
www.advmat.de

A Bottom-Up Approach to Red-Emitting Molecular-Based Nanoparticles with Natural Stealth Properties and their Use for Single-Particle Tracking Deep in Brain Tissue

Morgane Rosendale, Jessica Flores, Chiara Paviolo, Paolo Pagano, Jonathan Daniel, Joana Ferreira, Jean-Baptiste Verlhac, Laurent Groc, Laurent Cognet,* and Mireille Blanchard-Desce**

Fluorescent nanoparticles dedicated to bioimaging applications should possess specific properties that have to be maintained in the aqueous, reactive, and crowded biological environment. These include chemical and photostability, small size (on the scale of subcellular structures), biocompatibility, high brightness, and good solubility. The latter is a major challenge for inorganic nanoparticles, which require surface coating to be made water soluble. Molecular-based fluorescent organic nanoparticles (FONs) may prove a promising, spontaneously water-soluble alternative, whose bottom-up design allows for the fine-tuning of individual properties. Here, the critical challenge of controlling the interaction of nanoparticles with cellular membranes is addressed. This is a report on bright, size-tunable, red-emitting, naturally stealthy FONs that do not require the use of antifouling agents to impede interactions with cellular membranes. As a proof of concept, single FONs diffusing up to 150 μm deep in brain tissue are imaged and tracked.

Nanoparticles (NPs) benefit from a number of advantages over (free) fluorescent dyes including improved brightness[1] and longer vascular circulation times.[2] Inorganic NPs such as quantum dots (QDs)[3] and fluorescent polymeric NPs[4] are widely used for bioimaging applications. While QDs show remarkable brightness and photostability, they suffer from the intrinsic limitation of being water insoluble as bare nanomaterials, thus requiring coating by hydrophilic agents.[5] Moreover, the brightest QDs include toxic components (Cd, Se, As, In ...), which impede their applicability to translational research and raise concerns for environmental clearance.[6] An interesting alternative may thus lie with molecular-based fluorescent organic nanoparticles (FONs).[7] FONs are obtained by self-aggregation of dedicated dyes in water. Importantly, the properties of FONs can be finely tuned by molecular engineering of their constituting dyes. Redshifted emission of FONs made from dipolar or quadrupolar dyes is usually achieved by increasing the strength of the electron donor/acceptor pair or by excitonic coupling between dye subunits. However, we have previously reported on redshifted emission stemming from the nano-organization of dyes upon nanoaggregation.[8] We had indeed demonstrated that the emission of linear versus branched push–pull dipolar dyes was shifted from green to red in FONs, even though their fluorescence properties in organic solvents were virtually identical, indicating that the different imposed topologies of the subunits within nanoaggregates regulate their emission properties. Remarkably, redshifted FONs also revealed a markedly lower colloidal stability in the bloodstream than green-emitting ones, resulting in acute toxicity in vivo.[8] These founding results unveiled the promise that operating confinement-enhanced dipolar interactions and polarization effects can tune the luminescence properties, colloidal stability, and, most attractively, surface properties of FONs.[8,9] In this regard, a critical challenge specific to biomedical applications is to control the interactions between NPs and cells.[2,10] When subcellular compartments are to be targeted (e.g., for drug delivery), fluorescent nanoprobes should penetrate inside the cells. However, for detecting surface receptors (e.g., for diagnostics purposes) or exploring the extracellular space (ECS), they should remain outside the cells. A major field of research in which ECS exploration is currently gaining interest is neuroscience.[11] The ECS is indeed a key compartment that occupies 20–25% of the total brain volume, a fraction

Dr. M. Rosendale, J. Flores, Dr. P. Pagano, Dr. J. Daniel, Prof. J.-B. Verlhac, Dr. M. Blanchard-Desce
Institut des Sciences Moléculaires
CNRS
Univ. Bordeaux
Bordeaux INP, UMR 5255, 351 Cours de la Libération
Talence 33405, France
E-mail: mireille.blanchard-desce@u-bordeaux.fr
Dr. C. Paviolo, Dr. L. Cognet
LP2N
Institut d'Optique & CNRS
Univ. Bordeaux
UMR 5298, Rue François Mitterrand, Talence 33400, France
E-mail: laurent.cognet@u-bordeaux.fr
Dr. J. Ferreira, Dr. L. Groc
Interdisciplinary Institute for Neuroscience
CNRS
Univ. Bordeaux
UMR 5297, 146 Rue Léo Saignat, Bordeaux 33076, France
E-mail: laurent.groc@u-bordeaux.fr
The ORCID identification number(s) for the author(s) of this article can be found under https://doi.org/10.1002/adma.202006644.

DOI: 10.1002/adma.202006644

that varies with sleep, age, and disease.[12] The challenge for the development of NPs devoted to ECS exploration is to ensure the absence of nonspecific interactions with cellular membranes.[13] Surface coating or covalent grafting of poly(ethylene glycol) (PEG) chains are extremely popular strategies to yield stealth inorganic or polymeric NPs.[14] Surface modification however complicates the realization of a fully controlled nano–bio interface. Moreover, immunogenic responses to PEG moieties are increasing as these are more and more widely used in cosmetics and drugs.[15] In this work, we demonstrate an unusual approach to obtaining inherently stealth nanoparticles based on the specific structure of FONs constitutive dyes. Thanks to the unique combination of properties of the obtained FONs, i.e., brightness, redshifted emission, colloidal-, structural- and photostability, and above all intrinsic stealth behavior, we achieved deep tissue single-FON tracking in organotypic brain slices.

The design of the dye building blocks of these FONs is based on a quadrupolar scheme (D–π–A–π–D). A benzothiadiazole (BDTA) electron-withdrawing moiety is used as a potent central acceptor element (A) together with two propeller shaped electron-releasing diphenylamine moieties as donor end-groups (D) (**Figure 1**A,B).

Such a quadrupolar scheme promotes a periphery-to-core intramolecular charge transfer (ICT) which is accountable for strong absorption. ICT is also meant to influence the self-organization of dyes upon confinement: electrostatic interactions between quadrupolar dyes are expected to promote a specific packing as compared to dipolar dyes. In addition, we chose conjugated connectors made of fluorene moieties bearing two *n*-butyl side chains. This dye is thus herein named Q_{BDF}, for quadrupolar BDTA-diphenylamine-fluorene dye. The four alkyl chains extending above and below the plane of the fluorene units impose spacing between the dyes and are expected to hamper π–π interactions between fluorene moieties as well as hinder excitonic coupling.[16] They additionally convey a marked hydrophobic character, particularly at the edges of the molecule. Q_{BDF} is indeed well soluble in low to medium polarity organic solvents, shows very poor solubility in polar solvents, and is not soluble in water.

FONs made from Q_{BDF} are easily obtained by rapid addition of a minute amount of a stock solution of Q_{BDF} in tetrahydrofuran (THF) into a large volume of water (see Supporting Information). Nanoprecipitation proceeds readily with the quasi-instantaneous formation of a transparent and colored aqueous colloidal solution. The formation of nanoparticles of spherical shape can be attested by transmission electron microscopy (TEM) (Figure 1C, Figure S1A, Table S1, Supporting Information).

To examine the influence of NP size on their ability to diffuse into biological tissues, we modulated the FONs' size by varying the concentration of Q_{BDF} dye in THF prior to nanoprecipitation. Stock concentrations ranging from 0.4 to 4×10^{-3} M yield FONs of increasing sizes (**Table 1**) . Of note, the smaller FONs, nanoprecipitated from the lowest stock concentrations, show unimodal distributions with dry diameters averaging at 12 and 18 nm. In contrast, FONs originating from the more concentrated stock solutions show a bimodal distribution, yielding a mixture of two populations: very small FONs similar to the ones described above (≈15 nm), and bigger FONs of broader size dispersion (≈60 nm). Interestingly, all Q_{BDF} FONs show very negative surface potentials in water (Table 1).

Q_{BDF} FONs were found to be strong absorbers in the blue-green visible spectral region (Figure 1D, **Table 2**). The absorption spectra of dye subunits within FONs compare well with that of molecular Q_{BDF} in THF (Figure S2, Table S2, Supporting Information). Furthermore, no splitting or shoulder is observed, indicating a lack of excitonic coupling. The molar attenuation coefficient of Q_{BDF} FONs increases markedly with their size as is the case for QDs. Yet, their absorption spectra remain unchanged, indicating that their absorption originates from the absorption of individual dyes confined within the NPs and ruling out electron delocalization between subunits.

All Q_{BDF} FONs show bright fluorescence, illustrating the successful limitation of aggregation induced quenching within FONs. In contrast to QDs, their emission spectra remain

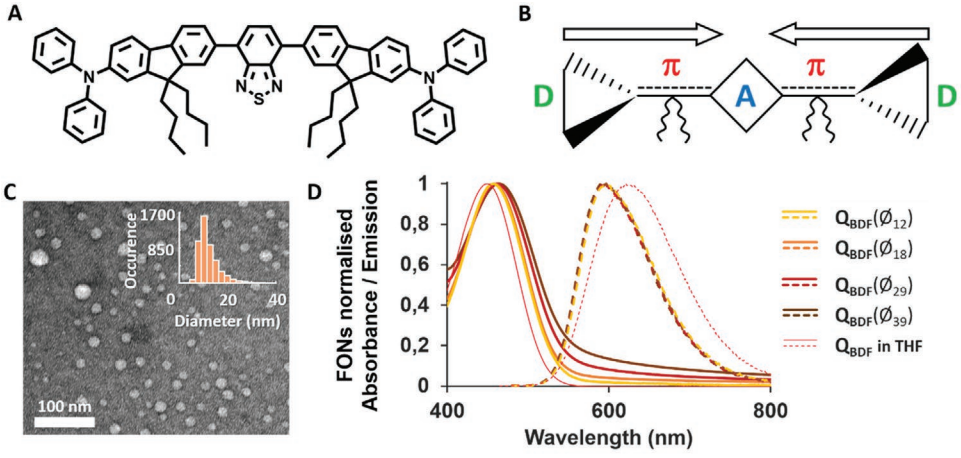

Figure 1. A) Chemical structure of the Q_{BDF} dye. B) Schematic of the D–π–A–π–D quadrupolar design. C) Representative transmission electron microscopy (TEM) image and size distribution (inset) of fluorescent organic nanoparticles (FONs) obtained by nanoprecipitation of 0.4×10^{-3} M Q_{BDF} dye in THF into water (1% v/v). D) Overlapped normalized absorbance (solid lines) and emission (dashed lines) spectra of Q_{BDF} dye in THF (red) and of Q_{BDF} FONs of different sizes (yellow to brown) prepared from varying dye stock concentrations in THF.

Table 1. Characteristics of Q_{BDF} fluorescent organic nanoparticles (FONs) of increasing size and comparison with red QDs.

NPs	$Ø_{TEM}$[a)] [nm]	$Ø_{SPT}$[b)] mQ [nm]	$Ø_{SPT}$[c)] PBS + FBS [nm]	ζ[d)] [mV]	N[e)]
Q_{BDF} (0.4×10^{-3} M)[f)]	12	57	72	−67	532
Q_{BDF} (1×10^{-3} M)[f)]	18	72	89	−64	1796
Q_{BDF} (2×10^{-3} M)[f)]	29	84	97	−64	7510
Q_{BDF} (4×10^{-3} M)[f)]	39	100	112	−63	18 266
QD605	10×3[g)]	–	–	–	–
QD655	12×5[g)]	22	–	–	–

[a)]Mean dry diameter determined by TEM; [b,c)]Hydrodynamic diameter determined by SPT in water (b) or by SPT in PBS + 10% FBS (c); [d)]Zeta potential; [e)]Average number of dye molecules per FON calculated from $Ø_{TEM}$; [f)]Stock concentration of Q_{BDF} dye used for nanoprecipitation is in parenthesis; [g)]Size measurements performed on images.[25] Red QDs are not purely spherical: approximate sizes are indicated as length x width.

virtually unchanged with increasing size (Figure 1D). Their fluorescence quantum yields, amounting to about 30%, are relatively high for bare, red-emitting NPs in water having no protective shell. We note that Q_{BDF} FONs show two distinct lifetimes in the ns range. The longer one is reminiscent of that of molecular Q_{BDF} in THF (5.5 ns, Table S2, Supporting Information) while the shorter might tentatively be ascribed to dyes located on the surface of the NPs as its contribution increases with decreasing size. These dyes may indeed undergo nonradiative (especially vibrational) decay processes favored by water molecules H-bonded to the surface.

Thanks to their intense absorption and sizeable fluorescence quantum yield, Q_{BDF} FONs show high brightness values, which increase significantly with size, in relation with the larger number of dyes confined within a single NP (Table 1, Figure S3, Supporting Information). Importantly, the brightness of the smallest FONs ($Q_{BDF}(Ø_{12})$) rivals that of red emitting QDs. Moreover, Q_{BDF} FONs show good colloidal stability. Colloidal suspensions may indeed vary in time such that NPs fuse or aggregate as the solution matures. Yet we observe that their absorption spectra remain virtually unchanged and show no increased scattering or broadening over a month (Figure S4, Supporting Information), and even up to 6 months (Figure S5, Supporting Information). This indicates that FONs neither aggregate nor agglomerate. Yet complementary measurements indicate that their size distributions slowly evolve over time (Figure S1B and Figure S6, Supporting Information) showing broadened size distributions. Interestingly, the bigger FONs ($Q_{BDF}(Ø_{39})$, $Q_{BDF}(Ø_{29})$) also maintain their fluorescence quantum yield over a month, while the smaller $Q_{BDF}(Ø_{18})$ and $Q_{BDF}(Ø_{12})$ respectively maintain 70% and 50% of their fluorescence over a month (Figure S5, Supporting Information). This suggests that slow surface rearrangements and exchange of the dyes from the surfaces of the NPs occur over time.

Based on the remarkable brightness of these FONs in aqueous medium, we evaluated their usability for single-particle tracking (SPT). We first assessed that they were photostable enough to remain detectable for around a minute under illumination (**Figure 2**A), an adequate time window to extract diffusion parameters.[17] We then detected FONs as freely moving puncta in water (Movies S1-S4, Supporting Information) whose Brownian motion could be tracked in post-acquisition image analysis (Figure 2B, Movie S5, Supporting Information), allowing us to determine the hydrodynamic diameter of FONs (Table 1, Table S3, Figure S7A, Supporting Information). In doing so, we made a thought-provoking observation: the hydrated diameters of Q_{BDF} FONs in water are substantially larger than their dry ones. This suggests the formation of a network of organized water molecules at the surface of FONs forming a polar, self-coating shell. Such behavior is reminiscent of the structuration of water molecules coating phospholipid bilayers.[18] Interestingly, we had previously reported a similar 50 nm increase in the hydrated diameter of FONs made from a different quadrupolar dye.[19] In contrast,

Table 2. Photophysical properties of Q_{BDF} fluorescent organic nanoparticle (FONs) of increasing size and comparison with red QDs.

NPs	λ_{abs}^{max}[a)] [nm]	ε^{max}[b)] [10^7 M^{-1} cm^{-1}]	λ_{em}^{max}[c)] [nm]	Φ_f[d)] [%]	τ_f[e)] [%]	$\varepsilon^{max}.\Phi_f$[f)] [10^6 M^{-1} cm^{-1}]
$Q_{BDF}(Ø_{12})$[g)]	458	1.4	598	29	4.6 (0.60) 1.9 (0.40)	4.0
$Q_{BDF}(Ø_{18})$	458	5.0	594	30	5.0 (0.62) 2.1 (0.38)	15
$Q_{BDF}(Ø_{29})$	462	21.2	595	33	5.5 (0.68) 2.6 (0.32)	70
$Q_{BDF}(Ø_{39})$	463	55.9	593	34	5.5 (0.69) 2.5 (0.31)	190
QD605[h)]	–	0.4	609	70	–	3.4
QD655[h)]	–	0.6	654	67	–	4.0

[a)]Absorbance maximum wavelength; [b)]Molar attenuation coefficient of the FONs at the absorbance maximum λ_{abs}^{max} considering N dye moieties per nanoparticle (Table 1); [c)]Emission maximum wavelength; [d)]Fluorescence quantum yield; [e)]Fluorescence lifetime. The contribution of each lifetime value to the fit is indicated between brackets; [f)]Brightness; [g)]Dry TEM diameter is in parenthesis; [h)]QDs absorb in the UV-vis with a sharp decrease after ≈500 nm. Here, ε^{max} was measured at λ_{abs}^{max} of $Q_{BDF}(Ø_{12})$ for comparison.

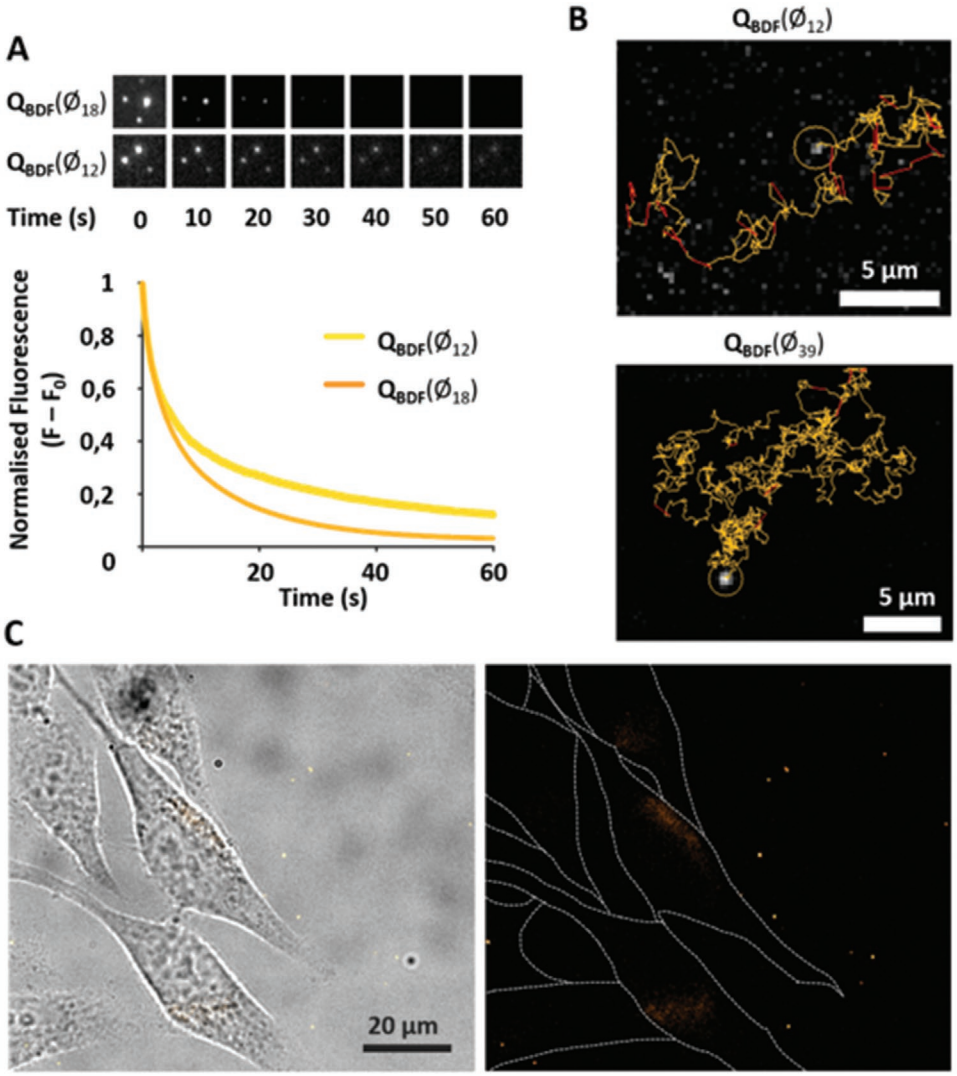

Figure 2. A) (Top) Example regions of interest and (bottom) average trace of Q_{BDF} fluorescent organic nanoparticles (FONs) intensity decaying with time. B) Example trajectory of a single $Q_{BDF}(Ø_{12})$ (top) and $Q_{BDF}(Ø_{39})$ (bottom) FON in water. C) Example fluorescence image of $Q_{BDF}(Ø_{18})$ FONs incubated for 24 h with HeLa cells: (left) overlaid with a bright-field image; (right) with cell contours traced for clarity.

we had reported that FONs composed of related dipolar[20] or bis-dipolar[21] dyes, bearing the same electron-donor moieties, displayed comparable dry and hydrated diameters. We next tracked FONs in phosphate buffered saline (PBS, pH 7.4, 310 mOsm) supplemented with 10% fetal bovine serum (FBS) (Table 1, Table S4, Figure S7B, Supporting Information) to investigate the possible formation of a protein corona. Interestingly, the presence of serum proteins generates a comparatively small increase in size, suggesting that the "ice" shell may buffer the direct interaction of the surface of FONs with proteins. Finally, we assessed the versatility of FONs under various pH and osmolarity conditions by confirming their integrity in two other physiologically relevant buffers: MES buffered saline (MBS, pH 5.5, 310 mOsm) used to mimick the acidic intravesicular environment and Artificial CerebroSpinal Fluid (ACSF, pH 7.4, 280 mOsm) routinely used for neuronal cultures, both supplemented with 10% FBS. We found that under either condition, FONs could be detected as punctate emitters of similar hydrodynamic diameter as in PBS + FBS (Table S5, Figure S8, Supporting Information).

Following on these results, we assessed the biocompatibility and observed the behavior of Q_{BDF} FONs in a cellular environment. We found that after 24 h incubation with HeLa cells in serum-containing culture medium, they did not stick to cell surfaces, indicating a lack of interaction with biological membranes (Figure 2C, Figure S9, Supporting Information). They also did not accumulate intracellularly, demonstrating that the specific Q_{BDF} dye design generates inherently stealth FONs that are not taken up by endocytosis. This behavior is rather unique in that the majority of FONs reported in the literature tend to be internalized by cells, including FONs made from dipolar[20,22] or quadrupolar[19,23] dyes having similar donor and/or acceptor groups. It is however reminiscent of recent reports on FONs made from bis-dipolar[21] or quadrupolar[24] dyes bearing fluorene-linked aliphatic pendant chains. Of note, most of those FONs also showed negative

surface potentials, indicating that the stealth behavior of Q_{BDF} FONs does not originate from the surface potential alone. This finding emphasizes the fact that the surface of a nanoparticle is crucial to its stealth behavior. As the specific bottom-up design of the dye tunes the nature of the interface between the FONs surface and the surrounding water molecules, the combination of the quadrupolar electronic charge distribution along the long axis and the presence, close to the edges of the dye, of long hydrophobic alkyl chains appears to be a determining factor. This finding unveils an original bottom-up route for engineering intrinsic stealth properties of FONs.

Considering the unique set of properties of bare Q_{BDF} FONs, we next investigated whether they could be used to explore the ECS of living tissues. We used hippocampal organotypic brain slices (**Figure 3**A) as a model system in which neuronal connectivity is partially maintained but where deep tissue imaging remains challenging. Recording depth is indeed critical in this system, as superficial layers of tissue may have reorganized after the slicing procedure. We focused our attention on the smaller FONs and observed that NPs of different sizes behave differently. After 2h incubation, $Q_{BDF}(Ø_{18})$ FONs could not satisfyingly penetrate inside the tissue. Most FONs were found near the surface of the slices and the few that were detectable at depth appeared immobile. In sharp contrast, $Q_{BDF}(Ø_{12})$ FONs were able to penetrate brain slices without excessively accumulating at the surface of the tissue, in a similar fashion to QD-655($Ø_{12x5}$), which we used for comparison (Movies S6,S7, Supporting Information). Moving QDs could reliably be imaged at various depths up to 80 µm. Under the same conditions, we recorded several freely moving $Q_{BDF}(Ø_{12})$ FONs up to 60 µm in depth as well as a few events past 80 µm and up to 150 µm deep (Figure 3B,C, Figure S10, Supporting Information). Hence, Q_{BDF} nanoparticles represent a new state-of-the-art nanotool for

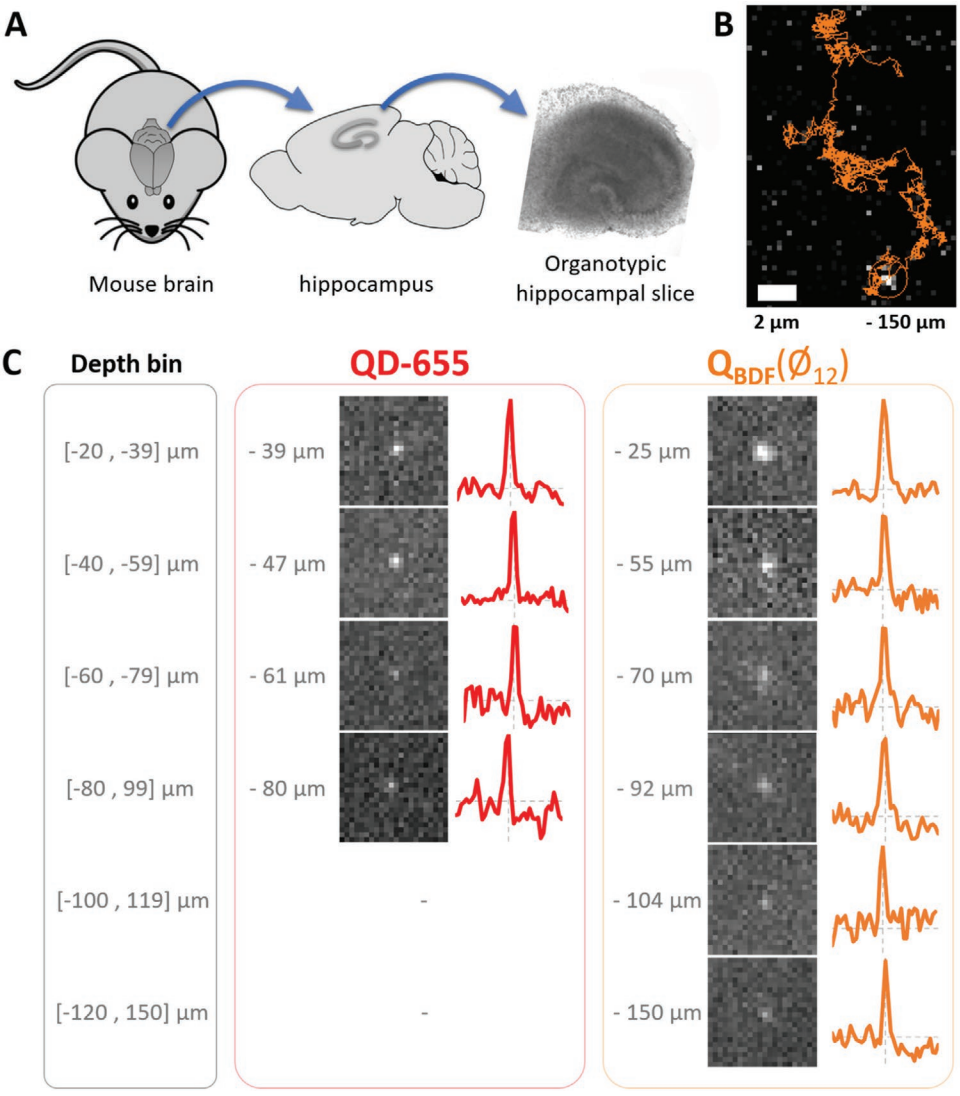

Figure 3. A) Schematic of organotypic brain slices preparation after extraction of the mouse brain and dissection of the hippocampus. B) Example trace of a $Q_{BDF}(Ø_{12})$ fluorescent organic nanoparticle (FON) recorded for 11 s, 150 µm below the surface of a brain slice. C) Example fluorescence images of QDs and FONs recorded at the indicated depths. To the right of each image, an intensity profile going from left to right of the brightest pixel is provided.

bioimaging deep in tissues, offering a non-toxic, eco-friendly alternative to heavy metal containing QDs.

We have therefore shown that stealth, bright, water-soluble, red-emitting, all organic nanoemitters of small size can be obtained by self-aggregation of specific quadrupolar dyes exhibiting strong ICT and decorated with four lipophilic pendant chains. Remarkably, the spontaneously stealth behavior of Q_{BDF} FONs is singular and contrasts with previous reports on FONS, including FONs made from dipolar and quadrupolar dyes that are used for intracellular imaging. Importantly, Q_{BDF} FONs require no PEG coating to achieve stealth behavior which simplifies the preparation of nanoprobes, reduces their complexity and allows greater control of their final size. Indeed, Q_{BDF} FONs can be made extremely small, down to ≈10 nm, i.e., roughly the size of an antibody, allowing for deep tissue imaging. Expanding our understanding of these FONs behavior in biological environments will be of the highest interest from a theoretical point of view, as the specific nature of the dye is obviously playing a major role. In particular, the intimate nature of the nanoparticle surface and sub-nanorugosity effects may be involved in the structuration of the nanointerface. Also, the technical feat of observing single spherical (0-D) nanoparticles more than 100 µm deep in tissue has seldom been reported. Further studies will be needed to systematically investigate whether at such depths, the ECS of the brain is influenced by various parameters such as local osmolarity, network excitability, or animal experience prior to brain slicing. Furthermore, the molecular design of FONs allows for finely tuned structural modifications such that several approaches can be envisaged for surface modification or biofunctionalization of these nanoparticles. These exciting possibilities will lead the way for safe, all organic bioimaging.

Supporting Information

Supporting Information is available from the Wiley Online Library or from the author.

Acknowledgements

This work received funding from the European Union's Horizon 2020 research and innovation program under the Marie Skłodowska-Curie grant agreement Nos. 841379 and 793296 to M.R. and C.P. J.F. was supported by the US-France-Belgium iREU Site in Translational Chemistry (NSF Grant No. 1560390). M.B-D. acknowledges support from Conseil Régional d'Aquitaine (Chaire d'accueil). The authors thank Agence Nationale de la Recherche (ANR-15-CE16-0004) and IdEx Bordeaux (ANR-10-IDEX-03-02). Transmission electron microscopy was done in the Bordeaux Imaging Center, a service unit of the CNRS-INSERM and Bordeaux University, member of the national infrastructure France Bioimaging (ANR-10-INBS-04). All procedures involving Sprague–Dawley rats were carried out in accordance with the guidelines of the University of Bordeaux/Centre National de la Recherche Scientifique Animal Care and Use Committee.

Conflict of Interest

The authors declare no conflict of interest.

Data Availability Statement

Research data are not shared.

Keywords

brain extracellular space, brightness, fluorescence, organic nanoparticles, single-particle tracking, stealth

Received: September 30, 2020
Revised: January 15, 2021
Published online:

[1] U. Resch-Genger, M. Grabolle, S. Cavaliere-Jaricot, R. Nitschke, T. Nann, *Nat. Methods* **2008**, *5*, 763.
[2] L. A. Lane, X. Qian, A. M. Smith, S. Nie, *Annu. Rev. Phys. Chem.* **2015**, *66*, 521.
[3] A. M. Wagner, J. M. Knipe, G. Orive, N. A. Peppas, *Acta Biomater.* **2019**, *94*, 44.
[4] Y. Braeken, S. Cheruku, A. Ethirajan, W. Maes, *Materials* **2017**, *10*, 1420.
[5] O. S. Wolfbeis, *Chem. Soc. Rev.* **2015**, *44*, 4743.
[6] T. L. Rocha, N. C. Mestre, S. M. T. Sabóia-Morais, M. J. Bebianno, *Environ. Int.* **2017**, *98*, 1.
[7] a) D. Svechkarev, A. M. Mohs, *Curr. Med. Chem.* **2019**, *26*, 4042; b) D. Horn, J. Rieger, *Angew. Chem., Int. Ed.* **2001**, *40*, 4330; c) S. Fery-Forgues, *Nanoscale* **2013**, *5*, 8428; d) W. A. Wani, M. Shahid, A. Hussain, M. F. AlAjmi, *Fluorescent Organic Nanoparticles: New Generation Materials with Diverse Analytical and Biomedical Applications*, Springer, Singapore, **2018**; e) E. Ishow, A. Brosseau, G. Clavier, K. Nakatani, P. Tauc, C. Fiorini-Debuisschert, S. Neveu, O. Sandre, A. Léaustic, *Chem. Mater.* **2008**, *20*, 6597.
[8] V. Parthasarathy, S. Fery-Forgues, E. Campioli, G. Recher, F. Terenziani, M. Blanchard-Desce, *Small* **2011**, *7*, 3219.
[9] a) C. Mastrodonato, P. Pagano, J. Daniel, M. Vaultier, M. Blanchard-Desce, *Molecules* **2016**, *21*, 1227; b) K. Amro, J. Daniel, G. Clermont, T. Bsaibess, M. Pucheault, E. Genin, M. Vaultier, M. Blanchard-Desce, *Tetrahedron* **2014**, *70*, 1903.
[10] a) L. Guerrini, R. A. Alvarez-Puebla, N. Pazos-Perez, *Materials* **2018**, *11*, 1154; b) R. L. Pinals, L. Chio, F. Ledesma, M. P. Landry, *Analyst* **2020**, *145*, 5090.
[11] a) R. G. Thorne, C. Nicholson, *Proc. Natl. Acad. Sci. USA* **2006**, *103*, 5567; b) S. Hrabetova, L. Cognet, D. A. Rusakov, U. V. Nägerl, *J. Neurosci.* **2018**, *38*, 9355.
[12] E. Syková, *Neuroscience* **2004**, *129*, 861.
[13] J. W. Shreffler, J. E. Pullan, K. M. Dailey, S. Mallik, A. E. Brooks, *Int. J. Mol. Sci.* **2019**, *20*, 6056.
[14] J. S. Suk, Q. Xu, N. Kim, J. Hanes, L. M. Ensign, *Adv. Drug Delivery Rev.* **2016**, *99*, 28.
[15] J. J. F. Verhoef, T. J. Anchordoquy, *Drug Delivery Transl. Res.* **2013**, *3*, 499.
[16] N. J. Hestand, F. C. Spano, *Chem. Rev.* **2018**, *118*, 7069.
[17] L. Groc, M. Lafourcade, M. Heine, M. Renner, V. Racine, J.-B. Sibarita, B. Lounis, D. Choquet, L. Cognet, *J. Neurosci.* **2007**, *27*, 12433.
[18] M. Prats, J.-F. Tocanne, J. Teissié, *Biochimie* **1989**, *71*, 33.
[19] J. Daniel, A. G. Godin, M. Palayret, B. Lounis, L. Cognet, M. Blanchard-Desce, *J. Phys. D: Appl. Phys.* **2016**, *49*, 084002.
[20] E. Genin, Z. Gao, J. A. Varela, J. Daniel, T. Bsaibess, I. Gosse, L. Groc, L. Cognet, M. Blanchard-Desce, *Adv. Mater.* **2014**, *26*, 2258.

[21] M. Rosendale, G. Clermont, J. Daniel, C. Paviolo, L. Cognet, J.-B. Verlhac, M. Blanchard-Desce, *Proc. SPIE* **2020**, *11360*, 1136005.

[22] a) A. Faucon, H. Benhelli-Mokrani, L. A. Córdova, B. Brulin, D. Heymann, P. Hulin, S. Nedellec, E. Ishow, *Adv. Healthcare Mater.* **2015**, *4*, 2727; b) D. Wang, H. Su, R. T. K. Kwok, X. Hu, H. Zou, Q. Luo, M. M. S. Lee, W. Xu, J. W. Y. Lam, B. Z. Tang, *Chem. Sci.* **2018**, *9*, 3685; c) J. Boucard, T. Briolay, T. Blondy, M. Boujtita, S. Nedellec, P. Hulin, M. Grégoire, C. Blanquart, E. Ishow, *ACS Appl. Mater. Interfaces* **2019**, *11*, 32808.

[23] J. Zhang, R. Chen, Z. Zhu, C. Adachi, X. Zhang, C.-S. Lee, *ACS Appl. Mater. Interfaces* **2015**, *7*, 26266.

[24] A. H. A. M. van Onzen, L. Albertazzi, A. P. H. J. Schenning, L.-G. Milroy, L. Brunsveld, *Chem. Commun.* **2017**, *53*, 1626.

[25] B. N. G. Giepmans, S. R. Adams, M. H. Ellisman, R. Y. Tsien, *Science* **2006**, *312*, 217.